Experimental and numerical investigation of thermoacoustic sources related to high-frequency instabilities

Mathieu Zellhuber[1], Joachim Schwing[1], Bruno Schuermans[2], Thomas Sattelmayer[1] and Wolfgang Polifke[1*]

[1]*Lehrstuhl für Thermodynamik, Technische Universität München, Boltzmannstr. 15, D-85748 Garching, Germany*

[2]*Alstom Power, CH-5401 Baden, Switzerland*

**Corresponding author: polifke@td.mw.tum.de*

(Submission date: February 22, 2013; Revised Submission date: June 12, 2013; Accepted date: July 31, 2013)

ABSTRACT

Flame dynamics related to high-frequency instabilities in gas turbine combustors are investigated using experimental observations and numerical simulations. Two different combustor types are studied, a premix swirl combustor (experiment) and a generic reheat combustor (simulation). In both cases, a very similar dynamic behaviour of the reaction zone is observed, with the appearance of transverse displacement and coherent flame wrinkling. From these observations, a model for the thermoacoustic feedback linked to transverse modes is proposed. The model splits heat release rate fluctuations into distinct contributions that are related to flame displacement and variations of the mass burning rate. The decomposition procedure is applied on the numerical data and successfully verified by comparing a reconstructed Rayleigh index with the directly computed value. It thus allows to quantify the relative importance of various feedback mechanisms for a given setup.

1. INTRODUCTION

The reduction of emissions of oxides of nitrogen has been at the core of development activities in gas turbine combustor technology for the past decades. This led to the widespread application of lean premix combustion concepts, which allow to limit the emission levels by avoiding the presence of fuel rich flame regions with high temperatures. However, lean premix systems are prone to thermoacoustic pulsations, which can appear from a positive coupling between heat release fluctuations and acoustic waves [1]. In consequence, thermoacoustic stability has become a central development objective for gas turbine combustor technology. Investigations were concerned predominantly with low-frequency, longitudinal and/or circumferential modes. Studies were conducted experimentally, analytically, and numerically; see e.g. [2–8].

The present work, on the other hand, is concerned with the stability of high-frequency acoustic modes with transverse components, which have received increased interest only recently in the gas turbine community. The physics of the flow-flame-acoustic feedback mechanisms are not yet well understood in this regime. Nevertheless, literature suggesting and discussing feedback mechanisms for jet and rocket engines dates back to the 1950s and 1960s. High-frequency instabilities in jet engine afterburners are described by Blackshear et al. [9], who reproduced the phenomenon in a generic test rig. Adiabatic compression and vortex-flame interaction are discussed as feedback mechanisms, but a quantitative model is not formulated. An interesting summary on the influence of design changes on high-frequency oscillations can be found in [10]. In the work of Barker [11] it is shown that the vortex shedding at the flame holder is acoustically induced, but a link between the vortices and the thermoacoustic feedback is not established. Blackman [12] investigated the location of the heat release, the total amount of heat released, and damping in the system with respect to high-frequency instabilities. Kaskan and Noreen [13] concluded from Schlieren images that the interaction of vortices and flame front are the key to understand the thermoacoustic feedback. However, this is partly revoked in the discussion attached to the same publication, since the link established by Kaskan and Noreen between oscillations, area change, and heat release fluctuations is based on assumptions that cannot be proven.

The experimental characterization of transversely excited swirled jets has been presented earlier by O'Connor and co-workers [14–16], Hauser et al. [17], and Worth and Dawson [18, 19] for the low-frequency range. High-frequency instabilities in swirl-stabilised flames were observed in the numerical works of Huang et al. [20, 21] and Huang and Yang [22], who gave a detailed description of the flame dynamics using proper orthogonal decomposition (POD) methods. Although they computed local distributions of the Rayleigh index, they did not discuss further on potential thermoacoustic feedback mechanisms that could drive the instabilities. A related non-compact analysis for longitudinal modes has recently been proposed by Leandro and Polifke [23] in the context of elongated flames.

As pointed out by Culick [24], it is generally acknowledged that periodic vortex formation can have a significant impact on combustion stability. However, no model has been developed yet that allows a general description of this feedback mechanism, thus its impact has to be investigated on a case-to-case basis. In this spirit, the present work develops means to identify and quantify the importance of thermoacoustic feedback mechanisms in the case of high-frequency transverse modes in gas turbine combustors.

The present study builds on two previous publications of Schwing and co-workers [25, 26], which describe the occurrence of self-excited, high-frequency transverse instabilities in a perfect premix swirl combustor. The main conclusion drawn from the extensive parameter variation reported in [26] is that "self-excited high-frequency instabilities can be observed at almost any parameter set when adjusting the air ratio" [26, p.3]. Hence, the authors put forward the hypothesis of a feedback mechanism that is constantly driving the transverse mode toward instability. They identified the periodic flame displacement by the acoustic velocity as such a driving feedback mechanism; the

same hypothesis was expressed by Méry et al. [27] with respect to transverse mode instabilities in rocket engines. Schwing et al. [26] further proposed a quantitative feedback model, which explicates how the periodic displacement of a flame with constant burning rate can cause a positive Rayleigh index. Zellhuber et al. [28] also studied high-frequency transverse instabilities in gas turbine combustors, by conducting large eddy simulations (LES) of an acoustically excited generic reheat combustor. Interestingly, the flame also showed a periodic displacement linked to acoustic velocity, and a globally positive Rayleigh index.

The present work first puts into perspective the previous results of Schwing et al. [26] and Zellhuber et al. [28]. At first sight, it might appear questionable to compare two different configurations that were investigated by different means. However, despite the differences in setup and methodology, both studies show a similar flame response to transverse acoustic modes, as follows from the qualitative comparison of the results presented in section 3. These similar observations of flame dynamics in distinct configurations stresses the need for a general understanding of the flame response to transverse acoustic perturbations. Therefore, the displacement feedback model of Schwing et al. [26] is further developed to a more general mathematical description of flame dynamics for transverse modes, including also contributions of non-constant burning rate (section 4.1). A tailored postprocessing of the numerical data is presented in section 5, in order to verify the validity of the proposed model and to quantify the relative importance of distinct feedback mechanisms.

2. FLAME CONFIGURATIONS AND INVESTIGATION METHODS

2.1 Experimental setup of swirl combustor

A swirl-stabilized flame is studied experimentally at atmospheric pressure. Air and fuel, i.e. natural gas, are perfectly premixed and the mixture is heated up to 673 K. Plenum, mixing tube, and cylindrical flame tube of the test rig are shown in Fig. 1. The diameter of the flame tube is 158 mm. Dynamic pressure sensors are used to identify mode shape and frequency. The test rig is equipped with an optical PIV measurement system, which records the Mie scattering of injected particles. Time-resolved, two- dimensional velocity fields are measured by comparing image pairs of particle distributions. The TiO_2 particles employed in the present work are not consumed by the flame.

The Mie scattering intensity is used as a qualitative indicator of the flow density at a certain location and is therefore inversely proportional to the local reaction progress [29, 30]. For the Mie scattering intensity, the image resolution is reduced in comparison to the PIV processing by a spatial average over neighbouring pixels. Hence, one can characterise local reaction progress fluctuations by processing time series of the Mie scattering intensity: The fluctuation amplitudes of scattering intensity and progress variable are proportional, while their phase signals are shifted by 180° with respect to each other.

More details on the setup can be found in [25] and [26].

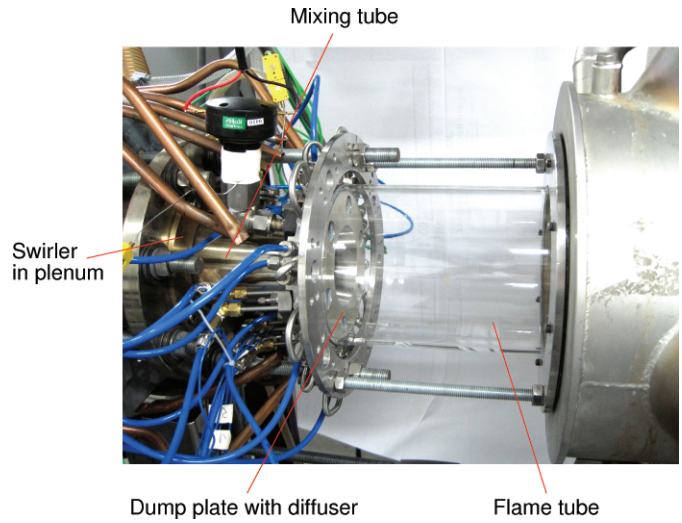

Figure 1: Experimental setup with swirler, mixing tube, and cylindrical flame tube.

2.2 Numerical setup of reheat combustor

The numerical part of the study was conducted on a generic reheat combustor at elevated pressure (p =18 bar) using Large Eddy Simulation (LES). The geometry is shown in Fig. 2 and consists of two coaxial cylindrical tubes of non-equal diameter, connected by a sudden jump in cross-sectional area. The diameter at the inlet is 80 mm, while a value of 2.5 was chosen for the area expansion ratio. The geometry has a total length of 250 mm. A perfect premixture of fuel (methane) and oxidiser (lean combustion products) with a mixture fraction of $Z = 0.01$ is injected at the inlet with a velocity of 55 m/s and a temperature of 1270 K. Due to the very lean conditions, the temperature rise over the flame is moderate, and thus leads to a relatively small density jump from the unburnt to the burnt region. The same configuration was considered by the authors in [28], where more detailed information is given on operating conditions.

Compressible LES was performed with the commercial software Fluent 13, using the coupled pressure-based solver. Temporal discretisation was set to second-order, spatial discretisation was performed with a second-order upwind scheme. A timestep of 3 µs was used throughout all simulations. Subgrid scale viscosity was modelled with a dynamic Smagorinsky approach.

The computational mesh consists of 1.16 million hexahedral elements, and includes refined layers close to the adiabatic duct walls and along the shear layer axis. In the shear layer region, the subgrid filter length lies within a range of 1.3 up to 3.4 times the laminar flame thickness obtained from 1D detailed chemistry calculations. The resulting LES quality index as defined by Celik et al. [31] ranges between 0.5 and 0.9 in the flame region. Lower values going down to 0.3 are only observed at the downstream part of the corner recirculation zone, and should not have a significant impact on the flame dynamics. The mesh independency of the presented results could

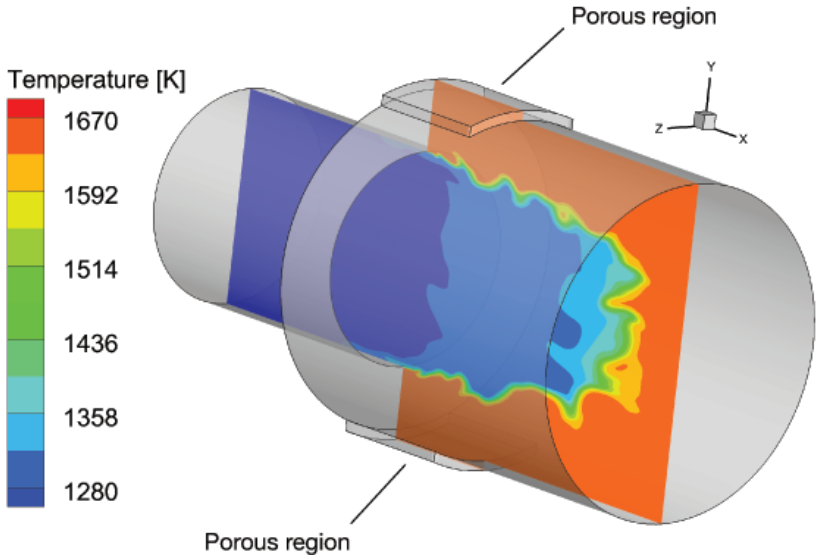

Figure 2: 3D view of simulated geometry with temperature distribution in symmetry plane

be verified by running additional simulations on finer meshes with 2.22 and 4.74 million cells. These yielded the same qualitative flame behaviour and comparable quantitative distributions of mean and fluctuation values as the ones shown in the present paper.

In order to ensure a stable stationary solution, non-reflecting boundary conditions were applied to inlet and outlet, using the state-space approach developed by Schuermans et al. [32]. The calculated inlet velocity was superposed with an inlet profile obtained from a separate RANS calculation, as well as with turbulent fluctuation terms, as obtained from the standard inlet turbulence generator in Fluent.

The combustion modelling is based on a composite progress variable approach making use of tabulated chemistry and Eulerian stochastic fields. The tabulation is based on homogeneous reactor calculations and detailed chemistry. The definition of the progress variable c , which includes intermediate as well as final product species, and a detailed description of the tabulation methodology can be found in [28]. For turbulence-chemistry interaction, the Eulerian Monte Carlo fields method [33] was used. It is based on a system of stochastic differential equations equivalent to the joint PDF evolution equations. The fields are continuous and differentiable in space and non-differentiable in time. This method of turbulence-chemistry modelling was successfully applied for autoignition simulations in LES with detailed chemistry [34–36]. In these works, a number of eight fields was judged to be sufficient when applying LES. For the present work, calculations were performed with 8 and 16 fields, and did not yield any

significative difference. All presented results correspond to the case of 8 fields.

In the general case treated in [37, 38], stochastic partial differential equations (PDE) are solved for progress variable and mixture fraction. However, the latter can be omitted for the present study due to the perfect premixing in order to save computational time. Hence, the following stochastic PDE is solved for the progress variable $c^{(n)}$ on each field:

$$\frac{\partial c^{(n)}}{\partial t} + u_j \frac{\partial c^{(n)}}{\partial x_j} = \frac{1}{\overline{\rho}} \frac{\partial}{\partial x_j} \left[\Gamma \frac{\partial c^{(n)}}{\partial x_j} \right] + \dot{\omega}^{(n)}_{c,chem} + \dot{\omega}^{(n)}_{c,stoch} - \dot{\omega}^{(n)}_{c,mix} \tag{1}$$

The formulation of the various source terms appearing in eqn (1) shall not be detailed here and can be found in [28]. The turbulence-chemistry interaction modelling consists in averaging the chemical source terms over the fields. The coupling between the stochastic and non-stochastic PDEs is made such that a fully compressible formulation is obtained. It shall be underlined that all tabulated chemistry data were generated at a constant reference pressure of 18 bar. The alteration of chemical reaction rates by acoustic pressure, as described by Ni et al. [39] and Zellhuber et al. [40, 41], is therefore excluded in the present study in order to focus on the remaining flame response mechanisms.

2.3 Acoustic excitation

In the swirl combustor experiment, self-excited, rotating 1T modes were identified as presented in [25]. The mode shape of a 1T mode in the flame tube calculated by a FEM solver is depicted in Fig. 3. The eigenfrequency of the first transverse mode varies with the flame shape, preheating temperature, and equivalence ratio, but is nearly independent of the mass flow rate [26]. In the experiments, it lies in the range of 3 kHz.

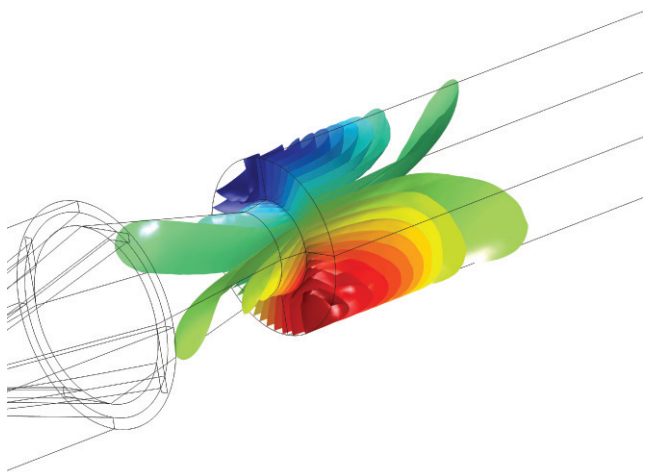

Figure 3: Mode shape in experimental setup estimated by FEM.

At low equivalence ratio, i.e. low thermal power, the system is always stable. Increasing the thermal power and the equivalence ratio, high-frequency instabilities occur [26]. The critical equivalence ratio, i.e. the point where the system changes from stable to unstable operation, is dependent on the swirl number, the preheating temperature, and the mass flow rate [26]. However, self-excited high-frequency instabilities occur in a wide range of operating conditions.

Contrary to the experimental setup, no self-excited instabilities appear in the simulation. Hence, in order to study the flame interaction with high-frequency modes, momentum source terms were applied in transverse direction within small porous zones located on top and bottom of the combustor (see Fig. 2). To force a specific mode type, one has to choose a suitable excitation frequency and source term direction. The frequency was estimated via acoustic mode calculations and/or FFT analysis of unexcited simulations, which can show distinct resonance peaks. The excitation direction simply depends on the mode type: the first transverse mode (1T) asks for an asymmetric excitation at top and bottom (same direction), whereas the second transverse mode (2T) is excited symmetrically, as illustrated in Fig. 4. A 1T mode was excited at a frequency of 3838 Hz, while a 2T mode appeared when exciting at 7450 Hz. Snapshots of the resulting pressure fields are also shown in Fig. 4. The axial variations of the 1T mode shape are not linked to longitudinal components, but are due to the varying cut-on-frequency along the axis, which depends on the tube diameter and the mean temperature. The 2T mode does on the contrary also contain longitudinal components, mainly upstream of the area expansion. The non-zero pressure amplitudes on the axis (2T case, see Fig. 4) appear since the excitation is only applied in one transverse direction.

The focus of the analysis made in the present work lies on the first transverse mode, as it was investigated in both experiment and simulation. However, the quantification procedure presented in section 5 will also be applied for the 2T mode in the simulation, in order to underline the general validity of the theoretical description proposed in section 4.1.

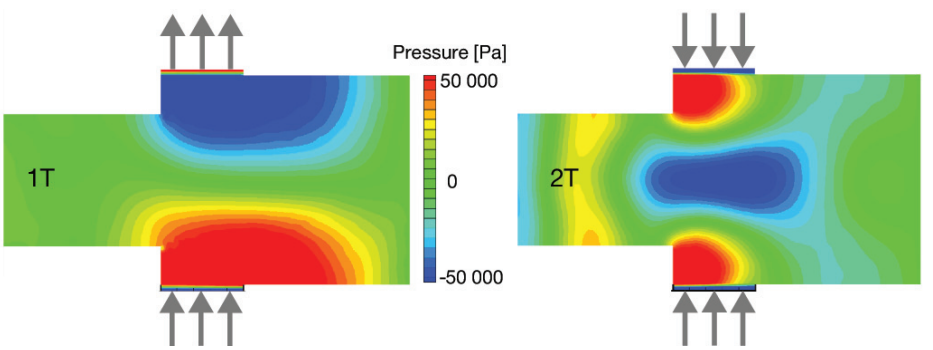

Figure 4: Orientation of momentum source terms used for the excitation of transverse modes; instantaneous snapshots of resulting pressure contours

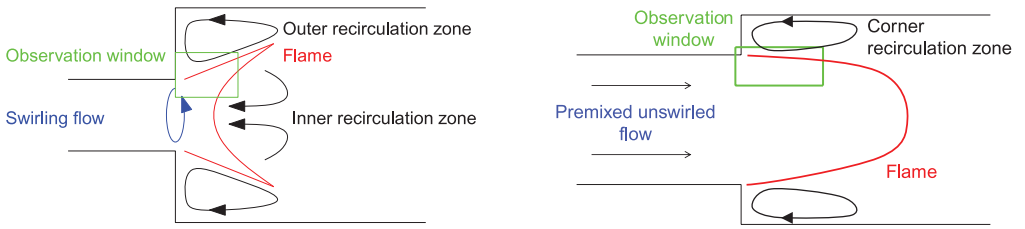

Figure 5: Sketches of swirl burner (experiment, left) and reheat burner (simulation, right), indicating also flame shape and observation window locations

3. QUALITATIVE COMPARISON OF OBSERVED FLAME DYNAMICS

The different burner configurations, flame shapes, and flow patterns of the experiment and the numerical simulation are sketched in Fig. 5. The experimental setup (left) is characterised by a swirled flow leading to an inner and outer recirculation zone and a M-shaped flame. The observation window used in the following is marked green and contains parts of the shear layers in the outer and inner recirculation zone. In the numerical calculations, the inlet flow is not swirled. Only a corner recirculation zone is formed, leading to the flame shape depicted in Fig. 5. Two characteristic flame regions can be discerned: a thin premix flame propagation zone in the shear layers and a quite homogeneous autoignition zone close to the burner axis (see [28]). The observation window contains the shear layer of the corner recirculation zone in the upper half.

When looking at temporal evolutions in both setups, as previously shown by the authors in [25] and [28], it appears that the flame response is strongly influenced by a periodic vortex formation at the burner exit. This results in high transverse velocity fluctuations in the shear layer and leads to a wrinkling of the flame front, which is transported in downstream direction at convective speed. Furthermore, it is apparent that the entire flame is periodically displaced in transverse direction at the acoustic frequency.

The overlay of these effects can be observed in amplitude and phase distributions of reaction progress fluctuations at the frequency of interest, which is either the instability frequency (self-excited case) or the forcing frequency (forced case). Therefore, a local analysis of progress variable fluctuations is performed via a Fast-Fourier-Transform (FFT) in swirl combustor experiment and reheat combustor simulation. For the latter, the FFT is applied in straightforward manner on the time series of reaction progress recorded in each computational cell. From there, one obtains an amplitude and a phase distribution of the fluctuations; the phase of the progress variable is given relatively to the phase of the pressure signal in the upper burner half. The same phase definition is chosen in the experiment. However, as mentioned earlier, the progress variable fluctuations are measured indirectly via the Mie scattering intensity. The FFT is therefore applied on the scattering intensity signal; the obtained amplitude is used as a qualitative measure of reaction progress amplitude, while the progress variable phase is obtained by adding $\pm 180^\circ$ to the phase of the Mie scattering intensity.

Alternatively, proper orthogonal decomposition (POD) and dynamic mode decomposition (DMD) could also be used for describing the flame dynamics. These tools are commonly employed for the identification of dominant flow structures. In a presentation of possible DMD applications, Schmid et al. [42] discuss the properties of POD, DMD, and Fourier analysis. For the simulation of a forced axisymmetric jet, they conclude that the additional information delivered by POD and DMD in comparison to a Fourier analysis is limited as the dominating frequency is known beforehand. Similarly, in the present work, the Fourier-based analysis is preferred, since the system dynamics in both configurations are dominated by a single frequency. Indeed, the application of POD to the reheat combustor simulation results did not deliver any additional information on overall flame dynamics. As pointed out by Schmid et al. [42], one might use DMD in order to get a very detailed understanding of the formation mechanisms of vortices and flame wrinkles close to the area expansion. However, this lies outside the scope of the present work; instead, it is more of interest to study how the resulting flame wrinkles affect the thermoacoustic flame response.

The amplitudes of progress variable fluctuations in the observation windows are shown in Fig. 6 for the two combustors. In both cases, high amplitudes can be identified in the shear layer region at the excitation frequency of the 1T mode; these are related to the varying position of the flame front. Moreover, a similar pattern can be recognised, with the alternation of high and low amplitude regions along the shear layer.

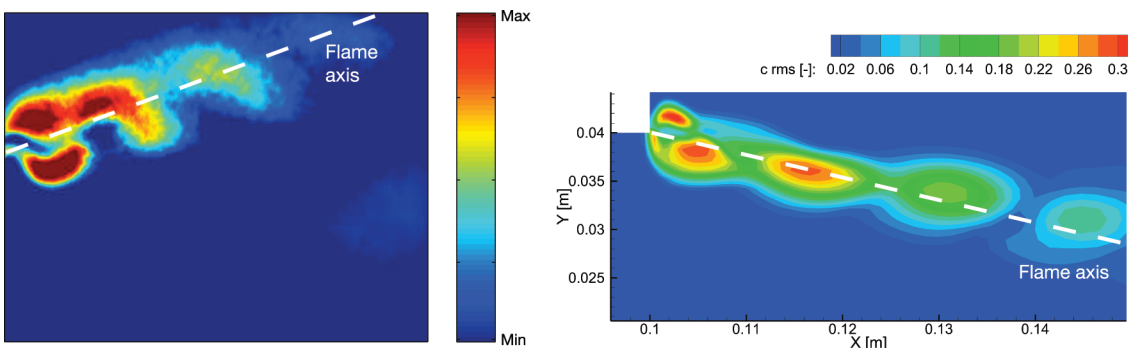

Figure 6: Qualitative amplitude distributions of progress variable fluctuations in swirl combustor experiment (left) and reheat combustor simulation (right) for 1T mode

Figure 7 shows phase distributions of progress variable for both configurations within the respective observation windows. For better clarity, the phase contours are shaded with the amplitudes, in order to show only regions with significant fluctuation levels. Looking at the swirl combustor experiment first, one can reckon two characteristic patterns: A rainbow colored region indicating a varying phase on the inner side of the shear layer and a large, red-colored region with a constant phase of ±180° on the outer side and at downstream positions. Only the rainbow pattern can be clearly

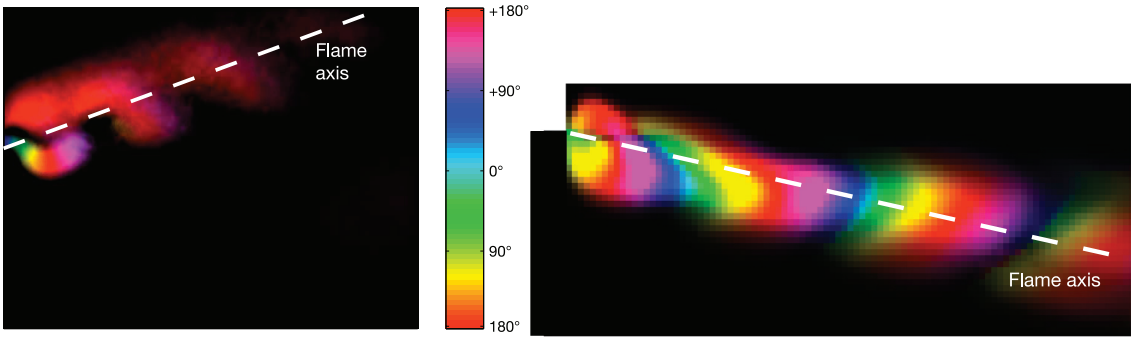

Figure 7: Amplitude weighted phase signal of progress variable fluctuations in swirl combustor experiment (left) and reheat combustor simulation (right) for 1T mode

distinguished within the observation window of the reheat combustor simulation. However, looking at the distribution in the entire flame tube shown in Fig. 9, a region with constant phase of ±180° also appears in the simulation at the downstream end of the upper shear layer.

These observations can be interpreted as follows: The rainbow pattern is caused by the periodic formation and downstream convection of flame wrinkles, as explained in the sketch of Fig. 8. The progress variable fluctuation signals at the two probe locations "a" and "b" are delayed with respect to each other, the delay being determined by the convection velocity. The corresponding phases will therefore be different, since the phase reference remains unchanged (pressure signal in upper burner half). If one extends this to more than two probes, the existence of a rainbow pattern becomes apparent.

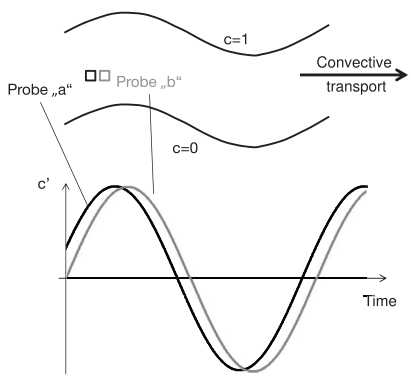

Figure 8: Sketch illustrating phase differences linked to convected flame wrinkles

The red-colored pattern at the downstream end is on the other hand caused by the periodic displacement of the flame due to acoustic velocity. Indeed, the flame displacement caused by the acoustics follows the transverse velocity fluctuation with a phase shift of 90˚ [26]. Hence, when the flame is at its uppermost position, the pressure is high, while the reaction progress in the shear layer is low. The resulting phase difference between reaction progress and pressure is 180˚ , and thus in accordance with the observations. The phase difference of 180˚ between the two shear layers in Fig. 9 comes from the fact that all phase values are given with respect to the pressure in the upper combustor half. In the swirl combustor experiment, this phase difference between the shear layers can be seen when comparing the outer and inner recirculation zone. Therefore, Fig. 10 shows the unshaded phase information. The inner shear layer is exposed to much more turbulent fluctuations, thus the intensity of the correlated signal is low. However, the blue colors dominate in the inner shear layer, and thus a phase difference of 180˚ to the outer one can be identified.

This shows that the reaction progress fluctuations and thus the displacement are due to both coherent flame wrinkling and transverse acoustic velocity. This overlay also causes the alternation of high and low amplitude regions that was observed in Fig. 6. A sketch explaining this pattern can be found in [28]. In the swirl combustor experiment, the flame wrinkles disappear after a short distance behind the area expansion; the constant phase region is hence dominating. In the reheat combustor simulation, however, the wrinkles travel a longer distance before being swept out, the constant phase region is thus located further downstream. In conclusion, despite the differences appearing in Fig. 7, the same characteristic patterns can be observed in both combustors.

It is further interesting to proceed to a comparison of fluctuation amplitudes for the transverse velocity and thus for the acoustic displacement. In the swirl combustor experiment, acoustic velocity fluctuations were measured by means of particle image

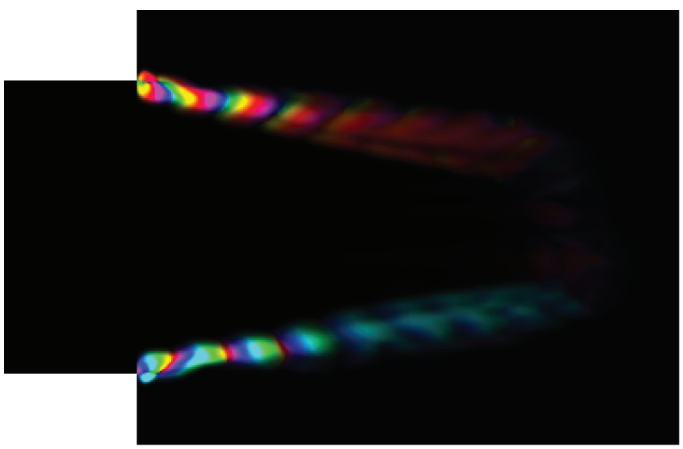

Figure 9: Amplitude weighted phase signal of progress variable fluctuations at excitation frequency for 1T mode (reheat combustor simulation).

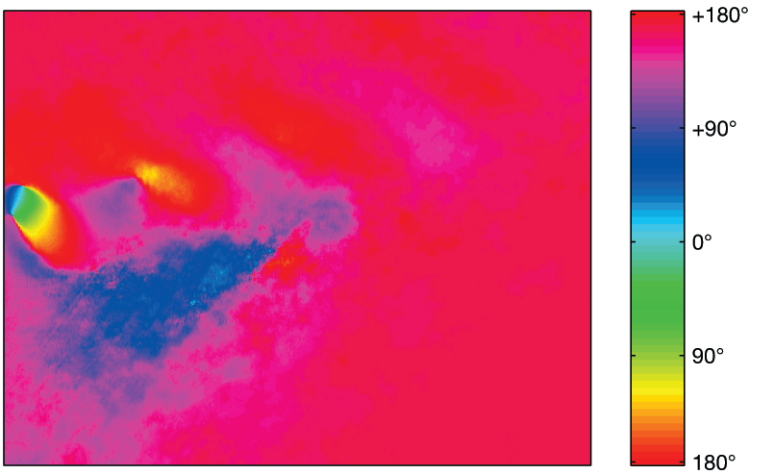

Figure 10: Phase signal of progress variable fluctuations at eigenfrequency of 1T mode (swirl combustor experiment).

velocimetry (PIV) [26]. In the shear layer between unburnt mixture and outer recirculation zone, the amplitude of the transverse velocity fluctuations at the eigenfrequency of the 1T mode is approximately $\hat{v} = 20$ m/s. The sinusoidal transverse velocity fluctuation $v'(t) = \hat{v} \cos(2\pi f t)$ leads to the expression for the transverse displacement $\Delta' = \int_0^t v'(\tau) d\tau = \hat{\Delta} \sin(2\pi f t)$. The amplitude of the displacement is $\hat{\Delta} = \hat{v}/(2\pi f) \approx 1$ mm. The amplitudes of acoustic velocity fluctuations and displacement are of the same order of magnitude in the reheat combustor simulation, with transverse velocity fluctuations of $\hat{v} = 10$ m/s at the shear layer position.

From this comparison, one can clearly recognise that the shear layer combustion shows in both cases a similar response to transverse acoustic excitation. The response can be summarised as a superposition of convectively transported, periodic flame wrinkling generated at the backward facing step and of transverse displacement due to acoustic velocity fluctuations. The overlay of these two effects leads to the characteristic patterns observed in the amplitude and phase distributions shown previously. In the following, it shall be explicated what this dynamic response represents in terms of thermoacoustic feedback. In [26], a model was proposed which quantifies the feedback caused by the acoustic transverse displacement. Considering the observations made, it is clear that the model needs to be extended in order to account for the wrinkling displacement, but also for fluctuations of the heat release rate, which will in any case occur because of the observed flame wrinkling.

4. CONTRIBUTIONS TO FLAME DYNAMICS

Fluctuations of heat release rate generally represent a concern for combustor stability, since they cause a thermoacoustic coupling, and might lead to an exponential growth of acoustic fluctuation amplitudes. Most often, this coupling is quantified using the

Rayleigh index RI, which relates fluctuations of volumetric heat release rate q' and pressure p' to each other:

$$\mathrm{RI} = \iiint \int_0^T p'(t,x,y,z)\,q'(t,x,y,z)\,dt\,dx\,dy\,dz. \tag{2}$$

A positive value of this Rayleigh index indicates a positive coupling between flame and acoustics, when the unsteady flame acts as an acoustic source. This holds true if the acoustic energy $e_{ac} = \bar{\rho}\,u_i'^2/2 + p'^2/(2\gamma\bar{p})$ is considered as the relevant disturbance energy for describing thermoacoustic instabilities. This assumption is widely used in industrial practice, when stability analysis of combustors is performed on the basis of the acoustic wave equation, using low-order network models, see e.g. Dowling [2], Schuermans et al. [43], Krüger et al. [44], or using 3D finite-element calculations, see e.g. Camporeale et al. [45].

The model presented in the following decomposes local heat release rate fluctuations into various contributions, whose relative importances regarding thermoacoustic coupling are assessed on the basis of the Rayleigh index. A possible application to alternative disturbance energy definitions is discussed in section 4.2.

4.1 Decomposition based on Rayleigh analysis

In the present section, an analytic description for the Rayleigh index is derived including various displacement effects and fluctuating heat release rates. In classical thermoacoustic theory, only the latter effect is generally taken into account when describing the feedback. Typical sources of heat release rate variations are modulations of flame surface, equivalence ratio, chemical kinetics, and density, see [43]. The feedback mechanism linked to acoustic displacement has only recently been introduced [26, 27] and can be nicely illustrated considering the observations made previously. The phase distributions showed that the flame reaches its uppermost position when the pressure is high in the upper half of the combustor. As a consequence, the flame is constantly shifted toward the positive pressure region and thus causes a positive global Rayleigh index even for a constant mass-burning rate. A graphical representation of this effect can be found altogether with the corresponding model description in [26]. Furthermore transverse displacement linked to flame wrinkles will also be considered in the present work. The feedback mechanism is similar as for the acoustic displacement, but it is not necessarily a driving mechanism, since the phase shift between displacement and pressure is varying, as indicated by the rainbow-coloured phase distributions.

The model extension made in the following is rather mathematical, but is based on the physical observations. It uses a Lagrangian perspective and introduces a moving frame which follows the local, total displacement field. As will be shown later, this representation allows to distinguish between temporal and spatial variations of the heat release rate, and thus to quantify separately the feedback produced by displacement and rate modulations. The volumetric heat release rate q can be written in the reference frame (x, y, z) as a mean quantity $\bar{q}$ plus fluctuations q'

$$q(x,y,z,t) = \overline{q}(x,y,z) + q'(x,y,z,t). \tag{3}$$

When considering only a single fluctuating frequency, the mean quantity can be defined as the average over one oscillation period:

$$\overline{q}(x,y,z) = \frac{1}{T}\int_0^T q(x,y,z,t)\,dt. \tag{4}$$

By changing from the reference frame to a moving frame ξ, ψ, ζ by the coordinate transform

$$x = \xi + \Delta_x(x,y,z,t), \tag{5}$$

$$y = \psi + \Delta_y(x,y,z,t), \tag{6}$$

$$z = \zeta + \Delta_z(x,y,z,t), \tag{7}$$

the heat release can be written in the moving frame

$$q_{\xi,\psi,\zeta} = \overline{q}_{\xi,\psi,\zeta}(\xi,\psi,\zeta) + q'_{\xi,\psi,\zeta}(\xi,\psi,\zeta,t). \tag{8}$$

Δ_x, Δ_y and Δ_z represent here the total displacement field, which in the context of the present work results mostly from the acoustic velocity and flame wrinkling. The mean quantity in the moving frame is defined as

$$\overline{q}_{\xi,\psi,\zeta}(\xi,\psi,\zeta) = \frac{1}{T}\int_0^T q_{\xi,\psi,\zeta}(\xi,\psi,\zeta,t)\,dt \tag{9}$$

by integrating in time in the moving frame. Applying the coordinate transform the time-dependent heat release is identical:

$$q(x,y,z,t) = q_{\xi,\psi,\zeta}(\xi,\psi,\zeta,t). \tag{10}$$

However, the mean quantities $\overline{q}$ and $\overline{q}_{\xi,\,\psi,\,\zeta}$ are different, as well as the fluctuating quantities $q' \neq q'_{\xi,\,\psi,\,\zeta}$.

The Rayleigh index for non-compact flames can be rewritten as follows:

$$\begin{aligned}\mathrm{RI} = \int_0^T\int_V p'(x,y,z,t)\,q'(x,y,z,t)\,dV\,dt &= \int_0^T\int_V p'(x,y,z,t)\,[q(x,y,z,t) - \overline{q}(x,y,z)]\,dV\,dt \\ &= \int_0^T\int_V p'(x,y,z,t)\,q(x,y,z,t)\,dV\,dt \\ &\quad - \int_0^T\int_V p'(x,y,z,t)\,\overline{q}(x,y,z)\,dV\,dt\end{aligned}$$

Fluctuations in heat release q' are expressed as a difference between the instantaneous heat release and the mean quantity. As the mean heat release is time-independent, the Rayleigh criterion can be written as

$$\begin{aligned}\mathrm{RI} = \int_0^T \int_V p'(x,y,z,t)\,q'(x,y,z,t)\,dV\,dt &= \int_0^T \int_V p'(x,y,z,t)\,q(x,y,z,t)\,dV\,dt \\ &\quad - \int_V \underbrace{\int_0^T p'(x,y,z,t)\overline{q}(x,y,z)\,dt}_{=0}\,dV \\ &= \int_0^T \int_V p'(x,y,z,t)\,q(x,y,z,t)\,dV\,dt.\end{aligned}$$

The relation between the heat release rate in the reference frame and in the moving frame can be written as follows:

$$\begin{aligned}q(x,y,z,t) &= q_{\xi,\psi,\zeta}(\xi,\psi,\zeta,t) \\ &= q_{\xi,\psi,\zeta}\left(x-\Delta_x(x,y,z,t), y-\Delta_y(x,y,z,t), z-\Delta_z(x,y,z,t), t\right)\end{aligned} \tag{11}$$

Introducing vector notation with $\vec{x} = \begin{pmatrix} x \\ y \\ z \end{pmatrix}$, $\vec{\Delta}_{\vec{x}} = \begin{pmatrix} \Delta_x \\ \Delta_y \\ \Delta_z \end{pmatrix}$, and the differential operator $\vec{\nabla} = \begin{pmatrix} \frac{\partial}{\partial x} \\ \frac{\partial}{\partial y} \\ \frac{\partial}{\partial z} \end{pmatrix}$ yields

$$q(\vec{x},t) = q_{\xi,\psi,\zeta}(\vec{x}-\vec{\Delta}_{\vec{x}},t) \tag{12}$$

$$\approx q_{\xi,\psi,\zeta}(\vec{x},t) - \vec{\nabla} q_{\xi,\psi,\zeta}(\vec{x},t)\cdot\vec{\Delta}_{\vec{x}}(\vec{x},t). \tag{13}$$

Splitting up the heat release rate into mean and fluctuating values in the moving frame, one obtains the relation

$$q(\vec{x},t) = \overline{q}_{\xi,\psi,\zeta}(\vec{x}) - \vec{\nabla}\overline{q}_{\xi,\psi,\zeta}(\vec{x})\cdot\vec{\Delta}_{\vec{x}}(\vec{x},t) + q'_{\xi,\psi,\zeta}(\vec{x},t) - \vec{\nabla} q'_{\xi,\psi,\zeta}(\vec{x},t)\cdot\vec{\Delta}_{\vec{x}}(\vec{x},t) \tag{14}$$

When neglecting higher order fluctuation terms, the last term on the R.H.S. of eqn (14) vanishes. Using this equation for the calculation of the Rayleigh index therefore leads to:

$$\begin{aligned} \mathrm{RI} &= \int_0^T \iiint p'(\vec{x},t)\, q(\vec{x},t)\, d\vec{x}\, dt \\ &= \underbrace{\int_0^T \iiint p'(\vec{x},t)\, \overline{q}_{\xi,\psi,\zeta}(\vec{x})\, d\vec{x}\, dt}_{=0} - \int_0^T \iiint p'(\vec{x},t)\, \vec{\nabla}\overline{q}_{\xi,\psi,\zeta}(\vec{x}) \cdot \vec{\Delta}_{\vec{x}}(\vec{x},t)\, d\vec{x}\, dt \end{aligned} \tag{15}$$

$$+ \int_0^T \iiint p'(\vec{x},t)\, q'_{\xi,\psi,\zeta}(\vec{x},t)\, d\vec{x}\, dt \tag{16}$$

$$= \underbrace{-\int_0^T \iiint p'(\vec{x},t)\, \vec{\nabla}\overline{q}_{\xi,\psi,\zeta}(\vec{x}) \cdot \vec{\Delta}_{\vec{x}}(\vec{x},t)\, d\vec{x}\, dt}_{=\mathrm{RI}_\Delta} + \underbrace{\int_0^T \iiint p'(\vec{x},t)\, q'_{\xi,\psi,\zeta}(\vec{x},t)\, d\vec{x}\, dt}_{=\mathrm{RI}_{q'}} \tag{17}$$

The flame feedback is therefore composed of two main contributions, one linked to periodic displacement movements of the flame RI_Δ and one linked to modulations of the heat release rate in the moving frame $\mathrm{RI}_{q'}$. Whereas the latter is commonly considered for low-frequency modes, the former has only recently come into the focus of thermoacoustic research [26, 27]. From the generally valid eqn (17), it becomes clear that significant feedback of displacement movements only occurs in regions with inhomogeneous mean heat release rate distributions.

A very convenient approximation can be made for the displacement contribution. The mean heat release rate in the (x, y, z) coordinate system may be used instead of the one in the (ξ, ψ, ζ) system. In fact, this introduces a small thickening of the mean flame shape due to the displacement, which will alter the distribution of the source term distribution at cell-scale, but will be of negligible effect when integrating over larger volumes. Hence, one may write

$$\mathrm{RI}_\Delta \approx -\int_0^T \iiint p'(\vec{x},t)\, \vec{\nabla}\overline{q}(\vec{x}) \cdot \vec{\Delta}_{\vec{x}}(\vec{x},t)\, d\vec{x}\, dt \tag{18}$$

Using this relation and knowing the mean flame distribution as well as the acoustic mode shape, one can thus easily obtain a good approximation of the source term contribution linked to the acoustic displacement.

In the previous work of Schwing et al. [26] the displacement contribution was expressed in a different form as

$$\mathrm{RI}_{\Delta,\text{Schwing et al.}} = \int_0^T \iiint p'(\vec{x}+\vec{\Delta}_{\vec{x}},t)\, \overline{q}(\vec{x})\, d\vec{x}\, dt. \tag{19}$$

This relation can be derived from the general case given by eqn. (18) by partial integration when one makes the assumption of a very thin flame in the direction of the

acoustic mode and hence of a constant displacement within the flame brush. This shall be explicated in the following for the simple two-dimensional example shown in Fig. 11. The displacement is assumed to occur only in y -direction, i.e. in transverse direction to the flame orientation. One can write for the displacement Rayleigh index in the area element $dA = (y_1 - y_0)dx$:

$$\mathrm{RI}_{\Delta,2\mathrm{D},\,\mathrm{thin}} = \int_0^T \int_{y_0}^{y_1} p'(x,y,t)\overline{q}(x,y)\,dxdydt - \int_0^T \int_{y_0}^{y_1} p'(x,y,t)\frac{\partial \overline{q}(x,y)}{\partial y}\Delta_y(x,y,t)\,dxdydt \tag{20}$$

Assuming a constant displacement $\Delta_y(x, y, t) \approx \Delta_y(x, t)$ over the flame front (thin flame assumption), the second term on the R.H.S. can be rewritten as follows when applying a partial integration:

$$-\int_0^T \int_{y_0}^{y_1} p'(x,y,t)\frac{\partial \overline{q}(x,y)}{\partial y}\Delta_y(x,y,t)\,dxdydt = -\int_0^T \Delta_y(x,t)\left[p'(x,y,t)\overline{q}(x,y)\right]_{y_0}^{y_1} dxdt + \int_0^T \Delta_y(x,t)\int_{y_0}^{y_1}\frac{\partial p'(x,y,t)}{\partial y}\overline{q}(x,y)\,dxdydt. \tag{21}$$

For the integral over a thin flame, as illustrated in Fig. 11, one reckons that $\overline{q}(x, y_0) = \overline{q}(x, y_1) = 0$ and hence $[p'(x, y, t)\,\overline{q}(x, y)]_{y_0}^{y_1} = 0$. The general expression for the Rayleigh index is therefore reduced to the one given by Schwing et al.:

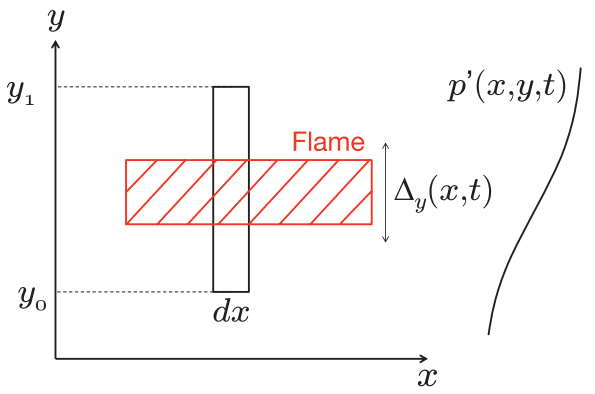

Figure 11: Simplified 2D configuration for Rayleigh index integration over a thin flame front

$$\mathrm{RI}_{\Delta,\mathrm{2D,\ thin}} =$$

$$\int_0^T \int_{y_0}^{y_1} p'(x,y,t)\overline{q}(x,y)\,dxdydt + \int_0^T \int_{y_0}^{y_1} \Delta_y(x,t)\frac{\partial p'(x,y,t)}{\partial y}\overline{q}(x,y)\,dxdydt \quad (22)$$

$$= \int_0^T \int_{y_0}^{y_1} p'(x,y+\Delta_y(x,t),t)\overline{q}(x,y)\,dxdydt. \quad (23)$$

From eqn (22), it follows that the displacement feedback for thin flames is proportional to the product of pressure gradient ($\alpha\ \omega$) and displacement ($\alpha\ \omega^{-1}$). The corresponding thermoacoustic source term is therefore likely to be approximately constant over the entire frequency range. The relevance of this feedback mechanism is therefore mainly dependent on the frequency scaling of the contributions linked to heat release modulations $\mathrm{RI}_{q'}$. The latter are often described by flame transfer functions showing a low-pass filter behaviour (see e.g. Huber et al. [46], Tay et al. [47]). One can thus postulate that displacement feedback is most likely to play a significant role at elevated frequencies. Hence, it is particularly important to take it into account when considering high-frequency transverse modes as it is the case for the present work.

A quantitative comparison of the various contributions will be done in section 5 using the numerical simulation data. The first term in eqn (17) denoting the feedback contribution of the total oscillatory displacement will then be further split up into contributions of acoustic velocity and flame wrinkling, which were identified in both experiment and simulation, see section 3. The acoustic displacement is of particular relevance, since it yields a throughout positive feedback contribution for thin flames, as explicated by Schwing et al. [26]. For the second term in eqn (17) one can as well proceed to a further decomposition, which may comprise modulations of flame surface, equivalence ratio, chemical kinetics, and density.

4.2 Comment on the wider applicability of the decomposition

In the present work, the Rayleigh index is employed as a measure of the thermoacoustic source term. Different authors indicated that the disturbance energy should also contain entropy fluctuations, in order to give a fully consistent definition of fluctuation budgets in reactive, non-isentropic flows. This issue was raised by Myers [48]. More recently, Nicoud and Poinsot [49], Giauque [50], Joseph George and Sujith [51, 52], as well as Brear et al. [53] further commented on this aspect. The latter work for instance proposed how to define a thermoacoustic source term for a disturbance energy containing entropy contributions. The proposed source term expression is far more complex than the Rayleigh index, as it contains many different terms.

The decomposition formalism introduced in the present work can also be applied to other definitions of thermoacoustic source terms. When looking at the derivation made above, it follows that eqn (17) is only based on a decomposition of the local heat release rate fluctuations into two distinct contributions. Any other fluctuation value in the flame could be decomposed in analogous manner, since the procedure is based on a kinematic description of flame displacement. Hence, the decomposition does not rely on the

Rayleigh index, which is used here only as a measure in order to compare the different feedback contributions. Their quantitative assessment presented in the following should therefore not be regarded as a generally valid quantification result, but as an example for a tailored analysis of thermoacoustic feedback in gas turbine combustors at elevated frequencies.

Regarding future work, it would be interesting to apply the decomposition to other thermoacoustic source term formulations. This would allow to discuss differences between acoustic energy norm definitions on the basis of practical flame configurations. With respect to industrial applications, it would be highly valuable to determine which energy convention allows the most accurate description of disturbance growth close to the combustor walls, which is the determining parameter for the mechanical integrity of the system. However, this discussion goes far beyond the scope of the present work.

5. QUANTIFICATION OF CONTRIBUTIONS TO THERMOACOUSTIC SOURCE TERM

Before comparing the various contributions with each other, the theoretical description proposed in the previous section and the approximations involved shall first be verified. Therefore, the various Rayleigh index contributions are quantified and the sum of these is compared to a direct computation of the Rayleigh index. As one can deduce from the equations presented, the quantification of the contributions asks for extensive amount of local flow data over sufficient time ranges. This amount of data can not be provided by the experimental diagnostics used in this work. As a consequence, the verification shall be performed on the simulation data gathered for the generic reheat combustor. There is no experimental validation available for this case; however, the comparison with the experimental results for the swirl burner showed a similar physical behaviour in both combustors.

The simulation offers the advantage of being able to access all needed flow data. Performing an analysis of the entire three-dimensional domain is unfortunately prohibitively expensive. Thus, only data in the central (x, y)-symmetry plane shown in Fig. 2 was post-processed, using the time-series of flow data at every grid point. The plane position was chosen such as maximum amplitudes appear in the observation domain. The results can thus be easily extrapolated to other planes by assuming lower fluctuation amplitudes.

5.1 Quantification methods: Evolution along shear layer

5.1.1 Reference: Direct computation of Rayleigh index

The distribution of the thermoacoustic source term within the observation plane shall first be considered. Such a volumetric Rayleigh index $\mathrm{ri}(x, y)$ can be calculated using its common definition, with the time series of pressure and heat release rate at each mesh element, which are bandpass-filtered around the excitation frequency:

$$\mathrm{ri}(x, y) = \int_0^T p'(x, y, t)\, q'(x, y, t)\, dt \tag{24}$$

The global Rayleigh index in the plane can simply be computed from the local one

by performing an area integration of the volumetric source term distribution.

For the present work, the integration shall however not be made over the entire area, but over distinct rectangular zones distributed along the shear layer, as shown in Fig. 12. Each zone of index i contains a surface A_i, representing a meso-scale observation window between the mesh scale size and the total flow domain scale. The high aspect ratio of the windows is chosen in order to ensure a high resolution in axial direction and to avoid that the flame moves out of the windows. The specific reasons for this choice are linked to the quantification of the single distributions and will be explained later. By resampling the Rayleigh index into the meso-scale windows, one obtains the evolution of the thermoacoustic source term along the shear layer. This resampling is made by a simple area integration of the volumetric source term distribution:

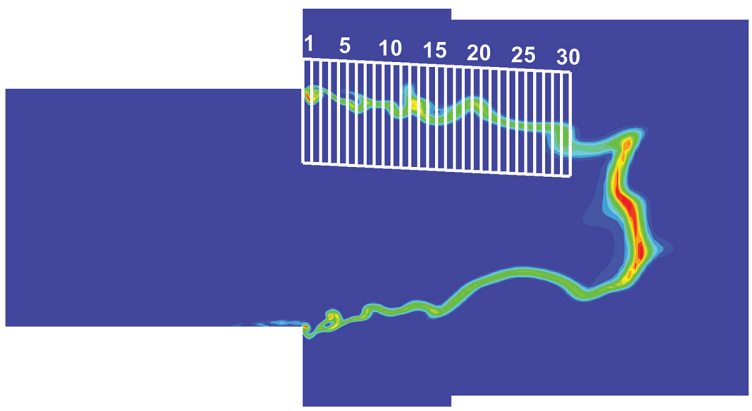

Figure 12: Definition of meso-scale windows along the shear layer

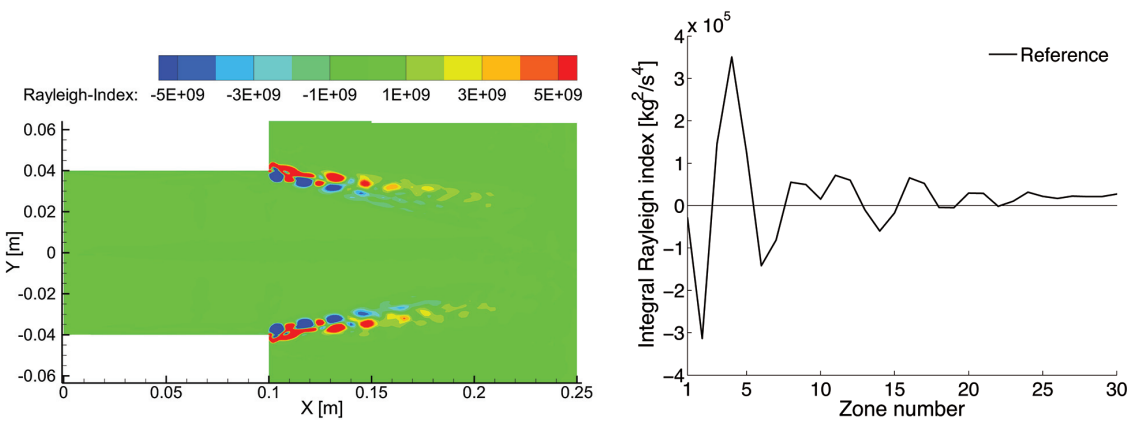

Figure 13: Left: Rayleigh index contours in the cutplane (see eqn 24), Right: Local Rayleigh index along the shear layer after resampling (see eqn 25)

$$\mathrm{RI}_i = \int_{A_i} \int_0^T p'(x,y,t) q'(x,y,t) dt dA = \int_{A_i} \mathrm{ri}(x,y) dA \tag{25}$$

The distributions of the Rayleigh index at the cell and at the meso-scale are shown in Fig. 13. One can observe an alternation of positive and negative regions in the vortex roll-up region, whereas a constant positive region appears further downstream. As explicated in [28] the jet core does not show any significant contribution to the source term, as the auto-ignition processes in the jet core are not modulated significantly by acoustic perturbations in the chosen simulation setup. It also clearly appears that the acoustic displacement does not lead to a significant feedback either, since the transverse gradient values of the mean heat release are very low in the auto-ignition zone.

The distribution shown on the right side of Fig. 13 will be used as reference data for the reconstruction of the Rayleigh index that will be presented in the following.

5.1.2 Displacement due to acoustic velocity

As introduced in [26, 27] and explicated in section 4.1, the displacement of a thin flame by the acoustic velocity field always contributes positively to the global thermoacoustic source term for high-frequency modes. For determining the magnitude of the feedback, it is necessary to calculate the corresponding acoustic displacement. Only displacement in y-direction is considered here; this is well suited to the 1T mode, but yields some difficulties regarding the T2 mode, as will be explained in more detail in section 5.2.

One therefore needs to separate between acoustic and wrinkling displacement contributions. This is done by first removing the rotational part from the filtered velocity field. Indeed, the acoustic velocity field can be considered as a pure potential field. However, the vortex roll-up at the burner exit will also induce rotational velocity components at the excitation frequency. These are not proper acoustic fluctuations, but result from the interaction of the acoustic perturbations with the mean flow. Hence, these shall not be included for the calculation of the acoustic displacement, but will be considered separately within a residual displacement that will be introduced later. The resulting potential velocity fluctuations in vertical direction v'_{pot} can be translated into a displacement by a time integration. When performing these operations on LES flow data, although most rotational components can be removed, the remaining velocity fluctuation distributions on the cell-scale are still not as smooth as typical distributions gained from purely FEM calculations. Therefore, an average acoustic displacement is calculated at the meso-scale for each observation window:

$$\Delta_{ac,i}(t) = \frac{1}{A_i} \int_{A_i} \int_0^t v'_{pot}(x,y,t) dt dA \tag{26}$$

Eventually, the resulting thermoacoustic source term contribution can be calculated. Using the approximation made for the derivation of eqn (18), the corresponding Rayleigh index reads as

$$\mathrm{RI}_{\Delta,ac,i} = -\int_{A_i}\int_0^T p'(x,y,t)\Delta_{ac,i}(t)\frac{\partial\overline{q}(x,y)}{\partial y}dtdA. \tag{27}$$

Using the average displacement on the meso-scale implies that the flame brush is thin with respect to the acoustic mode. This is indeed the case when looking at the shear layer. The original formulation of Schwing et al. [26], given by eqn (19), can therefore also be applied; the two expressions proved to be equivalent for the given case.

5.1.3 Displacement due to flame wrinkling

As mentioned earlier, there will also be additional displacement contributions to the acoustic one. It can be expected to originate mostly from flame wrinkling, but other effects might also play a role. For instance, flame speed variations might also lead to differences between the acoustic and the actual flame displacement. For this reason, it is generally referred to as a residual displacement. This displacement is quantified by calculating the difference between the actual and the acoustic displacement values.

The actual or total flame displacement is directly evaluated on the meso-scale level. Therefore, a spatially averaged reaction progress $c_i\ (t)$ is calculated for each window and every timestep:

$$c_i(t) = \frac{1}{A_i}\int_{A_i} c(x,y,t)dA. \tag{28}$$

Bandpass-filtering these time series around the excitation frequency and applying simple geometric considerations, one can express the total flame displacement in one window of height h_i as:

$$\Delta_{tot,i}(t) = -c_i'(t)h_i. \tag{29}$$

This result can be compared to the mean acoustic displacement in a window, as introduced in eqn (26). In regions of intense vortex roll-up, the total and the acoustic displacement are very likely to differ from each other. Hence, a residual displacement is introduced at window level, being defined as the difference between total and acoustic displacement values:

$$\Delta_{res,i}(t) = \Delta_{tot,i}(t) - \Delta_{ac,i}(t) \tag{30}$$

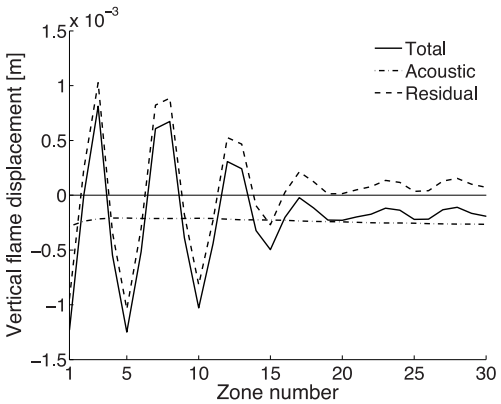

Figure 14: Displacement evolutions along the shear layer for 1T mode, given by the real parts of the corresponding FFT signal

Computing a Fourier transform at the excitation frequency of all three displacement signals for each window, one can directly compare them to each other, as shown in Fig. 14 for the real parts. The total displacement therefore appears to be strongly influenced by vortex roll-up close to the burner exit, whereas further downstream the acoustic displacement mostly prevails.

Assuming a constant residual displacement in a single window, the source term contribution of the residual displacement can now also be computed:

$$\mathrm{RI}_{\Delta,res,i} = -\int_{A_i}\int_0^T p'\left(x,y,t\right)\Delta_{res,i}\left(t\right)\frac{\partial\overline{q}(x,y)}{\partial y}dtdA \tag{31}$$

5.1.4 Heat release modulations due to density fluctuations

The Rayleigh criterion is based on the fluctuations of volumetric heat release rate. Hence, density variations will play a role, since more mixture will be located in regions of higher density. In the (x, y) coordinate system, variations of density $\rho'(x, y)$ result from the acoustic compression as well as from the displacement, since the density is varying over the flame front. In order to derive the variations in the (ξ, ψ) system, which are needed to compute $q'_{\xi,\psi}(x, y, t)$, a simplifying assumption is made, deriving the density variation directly from the pressure variation using the isentropic exponent. Indeed for isentropic state changes, one can write:

$$\frac{\rho'}{\overline{\rho}} \approx \frac{p'}{\gamma\overline{p}} \tag{32}$$

By using this approximation, the density variations caused by the periodic displacement are rendered insignificant, since they are of higher order, yielding the following expression for the respective source term contribution

$$\mathrm{RI}_{\rho,i} = \int_{A_i}\int_0^T p'(x,y,t)\frac{p'(x,y,t)}{\gamma\overline{p}(x,y)}\overline{q}(x,y)\,dt\,dA \tag{33}$$

Herein, the isentropic exponent γ is assumed to be constant over the flame front and equal to its value in the unburnt mixture. For the simulated flame, the variation of γ is below 2%, the assumption made is thus acceptable in the linear context.

5.1.5 Heat release modulations due to fluctuations of chemical consumption rates

The last considered contribution is related to variations of the chemical reaction rates, which can be derived by considering the mass specific heat release rate. Indeed, the spatial average of the mass-specific consumption rate in a window can be expressed as follows:

$$\dot{\omega}_i(t) = \frac{1}{A_i}\int_{A_i}\frac{q(x,y,t)}{\rho(x,y,t)}dA. \tag{34}$$

On the window-scale, such a mass-specific reaction rate can be affected in three ways, either by modulating the flame surface in the window, by modulating the local equivalence ratio, or by direct changes of the reaction rates, which can occur e.g. via the modelling of turbulence-chemistry interaction or the influence of acoustic pressure and temperature variations on the chemistry. The impacts of mixing and chemistry modulations is however not included in the present simulation setup, as the configuration is perfectly premixed and all tabulated chemistry data was generated at reference pressure.

The corresponding Rayleigh term contribution can thus be written as follows after bandpass-filtering the time series of $\dot{\omega}_i(t)$:

$$\mathrm{RI}_{\Delta} \approx -\int_0^T \iiint p'(\vec{x},t)\vec{\nabla}\overline{q}(\vec{x})\cdot\vec{\Delta}_{\vec{x}}(\vec{x},t)\,d\vec{x}\,dt \tag{35}$$

This term is generally considered as the dominant one for the feedback of compact flames, i.e. because of flame surface variations due to velocity fluctuations. The quantification results shown in the following section will elucidate whether the same conclusion holds for the feedback linked to high-frequency modes.

5.2 Results

Before comparing the different contributions among each other, the validity of the Rayleigh index decomposition shall first be verified. Therefore a comparison is made between the reference Rayleigh distribution as calculated in eqn (25) for the meso-scale windows and a reconstructed distribution, computed as the sum of the previously derived individual source term contributions:

$$\mathrm{RI}_{reconstr,i} = \mathrm{RI}_{\Delta,ac,i} + \mathrm{RI}_{\Delta,res,i} + \mathrm{RI}_{\rho,i} + \mathrm{RI}_{\dot{\omega},i}. \tag{36}$$

The result of the reconstruction is shown in Fig. 15 and proves to be very accurate when compared to the reference data. The procedure allows to properly capture the alternation of positive and negative regions in the vortex roll-up region, as well as the throughout constant source term distribution in the downstream part.

This characteristic pattern can be linked to the spatial distribution of the source term contributions, as shown in Figs. 16 and 17. Close to the burner exit, the Rayleigh index is strongly influenced by the intense flame wrinkling, which leads to locally high residual flame displacement, as well as to high fluctuations of the chemical consumption rates. The latter is of far higher importance for the local thermoacoustic source term, as the strong variations in the flame surface lead to intense coupling between the flame and the acoustics. However, it shall be underlined that for the 1T case, the two effects do not have as much an impact on the global thermoacoustic source term, because of the alternation of positive and negative contributions along the shear layer. In the downstream part, these two contributions are of very little impact even at the local scale, whereas the contributions of density fluctuations and acoustic displacement cause the constant positive Rayleigh index in this region. The constant positive sign of these two contributions is in agreement with theoretical expectations for thin flames.

By summing up the distinct contributions over the windows, one can get an appreciation of the relative importance of the different effects. The results are summarised in Fig. 18. These summed values highly depend on the considered locations. They should be handled with care, but do however allow some basic conclusions. Hence, the results clearly indicate that the acoustic displacement and the density contributions play the dominant roles for the 1T mode in the given case setup. The contribution of flame wrinkling, included in the residual displacement and reaction rate terms, is on the other hand slightly negative and relatively small when integrated over the entire flame, since the mentioned alternation of positive and negative regions

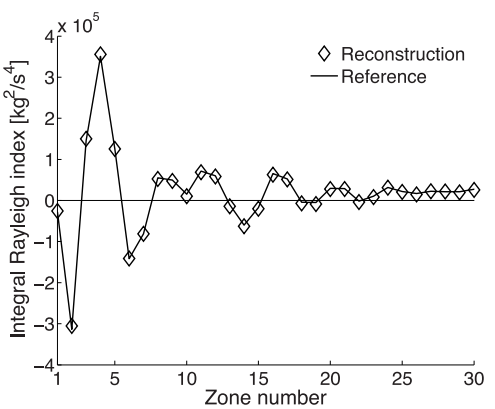

Figure 15: Comparison of reference and reconstructed Rayleigh indices along the shear layer for 1T mode

leads to a strong cancellation.

The application of the same analysis tools to the 2T excitation case shows as well a very good quality of the reconstruction, as shown in Figs. 18 and 19. This underlines the general applicability of the theoretical description proposed in section 4.1. Nevertheless, the relative importance of the individual contributions observed for the 1T mode in the simulation is different for the 2T excitation case. When looking at the individual curve evolutions and the summed values, it is observed that, contrary to the 1T mode, the contribution linked to the consumption rate and hence to the flame wrinkling now influences the global thermoacoustic source term more strongly. Physically, this can be explained by the smaller size of the vortices generated by the high-frequency 2T mode, due to the decreasing ratio between acoustic and convective timescale. The dissipation length of the vortices and hence the flame wrinkling is consequently shorter, what leads to a higher weighting of the region directly behind the area jump. As the latter shows a negative Rayleigh index, a stronger attenuating effect can be observed for the global contribution of the consumption rate, see Fig. 18. This is further aided by constantly negative values of this contribution in zones 1-15 and 20-30 (see Fig. 20), for which no clear explanation can be provided at present.

As mentioned, it is not possible to proceed to such a detailed quantitative comparison of the Rayleigh index contributions in the swirl burner experiment. However, as shown in detail in [54], it is possible to get an appreciation of the importance of the different effects, by a systematic variation of operating conditions (thermal power, fuel-air ratio), as well as by specific modifications of the burner geometry (swirl number, mixture distribution). It could be shown that the self-excited transverse instability observed in this setup is very likely to be mostly due to the acoustic displacement effect, as the strongest feedback was noticed in regions close to the velocity antinode.

The reader should not expect that it is possible to give a general assessment of the relative importance of the feedback mechanisms presented, as this is highly mode-dependent and also varies strongly over the spatial extent of a flame. Moreover, the relative importance of the mechanisms is supposed to depend as well on inlet and outlet boundary conditions, in particular when mixed modes with longitudinal components are involved; however, this aspect has not been investigated yet. In general, the identification of predominant feedback mechanisms has to be carried out on a case-to-case basis.

Nevertheless, the analysis made on the numerical data could verify the decomposition presented in section 4.1 and thus confirm the relevance of the supposed feedback mechanisms. These can generally be split into two different kinds:

1. Inherent contributions: acoustic displacement and density. These contributions always appear and can be predicted easily from the mean flame shape and the acoustic mode structure. The corresponding feedback is always positive for the density; the same applies to the acoustic displacement when the flame brush is thin in direction of the acoustic mode. For homogeneous reaction zones, like the auto-ignition zone in the numerical setup, the feedback linked to acoustic displacement is typically rather low. Under given circumstances, it can also become negative depending on the distribution of the mean heat release rate.

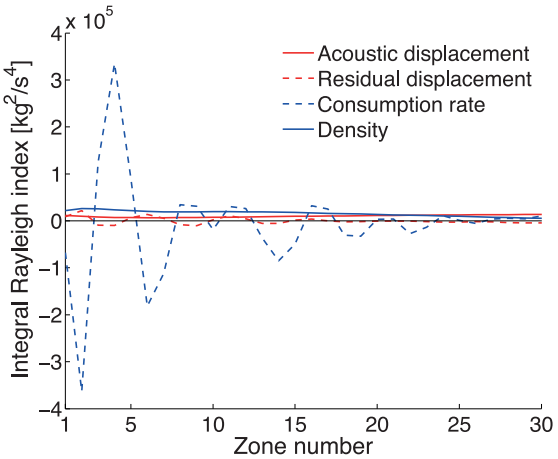

Figure 16: Respective contributions to the local Rayleigh index along the shear layer for 1T mode

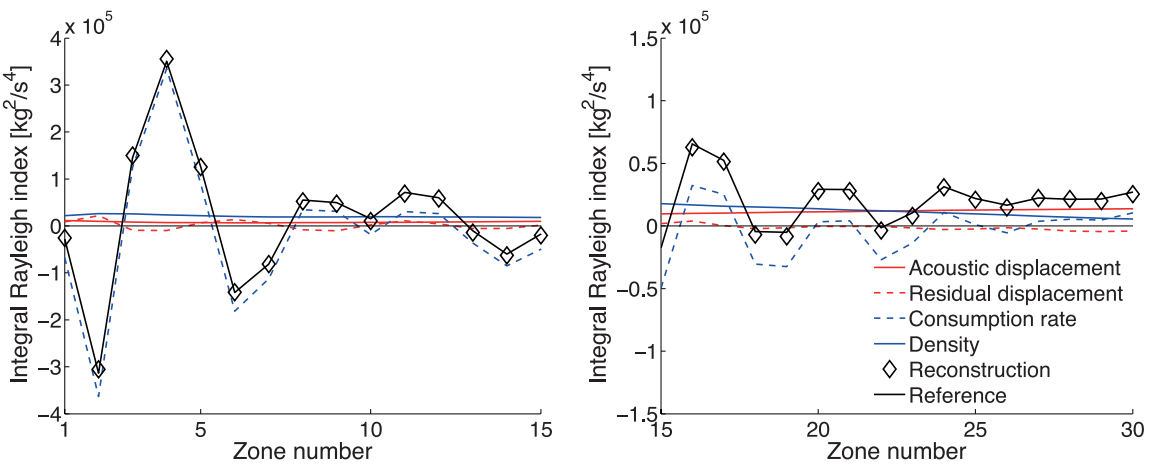

Figure 17: Respective contributions to the local Rayleigh index along the shear layer for 1T mode, enlargement of upstream (left) and downstream windows (right)

The impact of these inherent contributions can only be influenced by modifying the global fame shape, either by modifying its position with respect to the acoustic mode or by generating homogeneous reaction zones minimising the acoustic displacement feedback.

2. Varying contributions: residual displacement and consumption rate. Their effect will depend on the case setup and the excitation frequency, and can be

of dampening or forcing character. A beforehand prediction is difficult, as it strongly depends on the vortex roll-up and flame wrinkling. Nevertheless, this offers the possibility to reduce the global source term by design means aimed at influencing locally the vortex roll-up at the burner exit.

The presented quantification method allows to give a prediction of the influence of the different effects from Large-Eddy-Simulations for a single mode. Regarding the high number of modes existing in the respective frequency range in a full annular

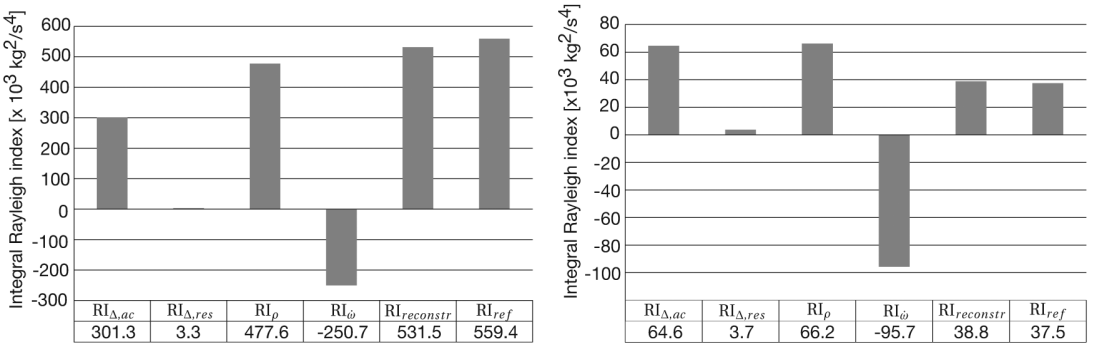

Figure 18: Quantification of different contributions to the Rayleigh index, summed up over mesoscale windows ($RI = \Sigma_i RI_i$). Relative overall error of the reconstruction is –5 % for the T1 mode (left) and 4 % for the T2 mode (right).

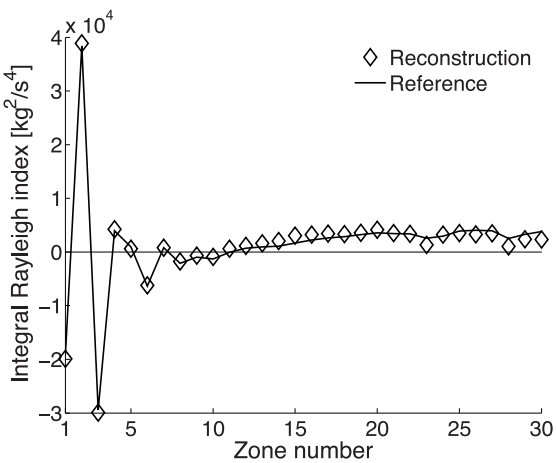

Figure 19: Comparison of reference and reconstructed Rayleigh index evolution along the shear layer for 2T mode

combustor, this method would turn out to be far too expensive for use in the design for stability of industrial gas turbines, but it can deliver some valuable insight into the physical mechanisms that lead to thermoacoustic instabilities, as done in the present work.

6. CONCLUSIONS AND OUTLOOK

Experimental and numerical observations of high-frequency instabilities showed a similar response of two different types of flames to transverse acoustic excitation. In both cases, the flame was subjected to transverse displacement movements caused by the acoustic velocity and to wrinkling by the coherent vortex formation at the area expansion. From qualitative observations only it is not possible to draw conclusions on the feedback mechanism mainly responsible for the occurrence of instabilities.

Therefore, an extended theoretical model is proposed: It consists in a decomposition of the thermoacoustic source term into distinct contributions, which can be associated with the observed physical effects. The model allows to gain a much better insight into transversal high-frequency instabilities, as it describes the interplay between the potential feedback mechanisms.

In order to verify the model, the total thermoacoustic source term is reconstructed from the distinct contributions for the numerical case. The reconstruction was done using a tailored post-processing of the simulation data and yields excellent agreement with the directly calculated Rayleigh index. Though, the respective contributions of the different effects could be quantified for the numerical setup. The results indicate that the relative importance of the effects highly depends on the considered case, ruling out any generally

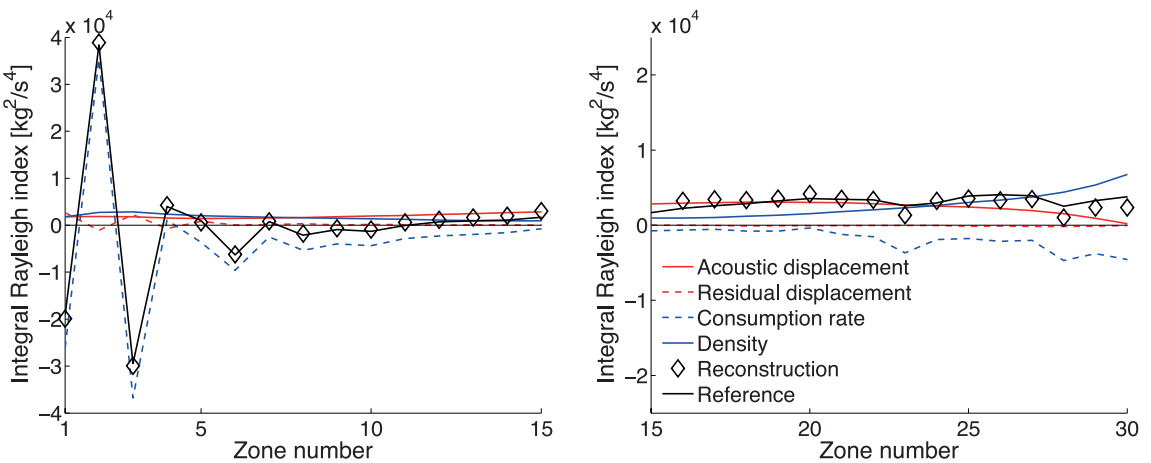

Figure 20: Respective contributions to the Rayleigh index evolution along the shear layer for 2T mode, enlargement of upstream (left) and downstream windows (right)

valid conclusion regarding the dominant feedback mechanism for transverse instabilities. Nevertheless, the present work provides the theoretical foundation for analysing thermoacoustic feedback related to high-frequency transverse modes. Building up on this knowledge, it is possible to determine the dominating effect also by other ways than using the presented reconstruction method, e.g. by systematic geometry and operation point variations, as done for the investigated premix swirl combustor in [54].

In the future, the presented model requires additional confirmation, e.g. by performing compressible LES of the premix swirl combustor and applying the decomposition procedure to its results. Moreover, it would be beneficial to find a way to adopt the reconstruction procedure on the basis of detailed experimental data. This could then be used for an in-depth validation of the employed numerical simulation techniques. Note, however, that this requires extremely demanding, time and space-resolved diagnostics of pressure, velocity and heat release rate. The simulation, on the other hand, should be extended with respect to the pressure sensitivity of chemical reaction rates, in particular when dealing with auto-ignition flames. Fortunately, such an extension of the combustion model presents no essential difficulty [40].

7. ACKNOWLEDGEMENTS

The authors would like to acknowledge the funding provided by the State of Bavaria and Alstom in the framework of the German research initiative KW21 II (subprojects BY13GV and BY16GV).

REFERENCES

[1] Lord Rayleigh. The explanation of certain acoustical phenomena. *Nature*, 1878, 18(455):319–321.

[2] A. P. Dowling. The calculation of thermoacoustic oscillations. *Journal of Sound and Vibration*, 1995, 180(4):557–581.

[3] W. Polifke, C. O. Paschereit, and K. Döbbeling. Constructive and Destructive Interference of Acoustic and Entropy Waves in a Premixed Combustor with a Choked Exit. *Int. J. of Acoustics and Vibration*, 2001, 6(3):135–146.

[4] B. Schuermans, V. Bellucci, and C. O. Paschereit. Thermoacoustic modeling and control of multi burner combustion systems. In *Proceedings of ASME Turbo Expo 2003-GT-38688*, 2003.

[5] T. Sattelmayer. Influence of the combustor aerodynamics on combustion instabilities from equivalence ratio fluctuations. *J. of Engineering for Gas Turbines and Power*, 2003, 125(1):11–19.

[6] G. Staffelbach, L. Y. M. Gicquel, G. Boudier, and T. Poinsot. Large eddy simulation of self excited azimuthal modes in annular combustors. *Proceedings of the Combustion Institute*, 2009, 32(2):2909–2916.

[7] T. Komarek and W. Polifke. Impact of swirl fluctuations on the flame response of a perfectly premixed swirl burner. *J. Eng. Gas Turbines Power*, June 2010, 132(6):061503–1,7.

[8] P. Palies, D. Durox, T. Schuller, and S. Candel. The combined dynamics of

swirler and turbulent premixed swirling flames. *Combustion and Flame*, September 2010, 157(9):1698–1717.

[9] P. L. Blackshear, W. D. Rayle, and L. K. Tower. Experimental determination of gas motion accompanying screeching combustion in a 6-inch simulated afterburner. Technical Report RM E53I28, National Advisory Committee for Aeronautics, 1953.

[10] Lewis Laboratory. A summary of preliminary investigations into the characteristics of combustion screech in ducted burners. Technical report, National Advisory Committee for Aeronautics, 1954.

[11] C. L. Barker. *Experiments concerning the occurence and mechanism of high-frequency combustion instability*. PhD thesis, California Institute of Technology, Pasadena, California, 1958.

[12] A. W. Blackman. Studies of screeching combustion and pressure-wave, flamefront interaction. *Combustion and Flame*, 1961, 5:175–190.

[13] W. E. Kaskan and A. E. Noreen. High-frequency oscillations of a flame held by a bluff body. *Transactions of the American Society of Mechanical Engineers*, 1955, 77:885–895.

[14] J. O'Connor, S. Natarajan, M. Malanoski, and T. Lieuwen. Disturbance field characteristics of a transversely excited annular jet. In *Proceedings of ASME Turbo Expo, GT2010-22133*, Glasgow, UK, 2010. ASME.

[15] J. O'Connor and T. Lieuwen. Disturbance field characteristics of a transversely excited burner. *Combustion Science and Technology*, 2011, 183:427–443.

[16] J. O'Connor and T. Lieuwen. Further characterization of the disturbance field in a transversely excited swirl-stabilized flame. *Journal of Engineering for Gas Turbines and Power*, 2012, 134:1–9.

[17] M. Hauser, M. Lorenz, and T. Sattelmayer. Influence of Transversal Acoustic Excitation of the Burner Approach Flow on the Flame Structure. *Journal of Engineering for Gas Turbines and Power*, 2011, 133(4):041501/1–8.

[18] N. A. Worth and J. R. Dawson. Cinematographic oh-plif measurements of two interacting turbulent premixed flames with and without acoustic forcing. *Combustion and Flame*, March 2012, 159(3):1109–1126.

[19] N. A. Worth and J. R. Dawson. Self-excited circumferential instabilities in a model annular gas turbine combustor: Global flame dynamics. *Proceedings of the Combustion Institute*, 2013, 34(2):3127–3134.

[20] Y. Huang, H.-G. Sung, S.-Y. Hsieh, and V. Yang. Large-eddy simulation of combustion dynamics of lean-premixed swirl-stabilized combustor. *Journal of Propulsion and Power*, 2003, 19:782–794.

[21] Y. Huang, S. Wang, and V. Yang. Systematic analysis of lean-premixed swirl-stabilized combustion. *AIAA Journal*, 2006, 44:724–740.

[22] Y. Huang and V. Yang. Dynamics and stability of lean-premixed swirl-stabilized combustion. *Progress in Energy and Combustion Science*, 2009, 35:293–364.

[23] R. E. Leandro and W. Polifke. Low-order modelling of distributed heat release. In *Proceedings of 19th International Congress on Sound and Vibration (ICSV19), Vilnius, Lithuania*, 2012.

[24] F. E. C. Culick. *Unsteady Motions in Combustion Chambers for Propulsion Systems*. Number AC/323(AVT-039)TP/103 in RTO AGARDograph AG-AVT-039. 2006.

[25] J. Schwing, N. Noiray, and T. Sattelmayer. Interaction of vortex shedding and transverse highfrequency pressure oscillations in a tubular combustion chamber. In *Proceedings of ASME Turbo Expo, GT2011-45246*, Vancouver, Canada, 2011. ASME.

[26] J. Schwing, F. Grimm, and T. Sattelmayer. A model for the thermo-acoustic feedback of transverse acoustic modes and periodic oscillations in flame position in cylindrical flame tubes. In *Proceedings of ASME Turbo Expo 2012, GT2012-68775*, 2012.

[27] Y. Méry, L. Hakim, P. Scouflaire, L. Vingert, S. Ducruix, and S. Candel. Experimental study of the combustion-acoustics coupling in liquid rocket engine high-frequency instabilities. In *Proceedings of AAAF-ESA-CNES Space Propulsion 2012*, Bordeaux, France, 2012.

[28] M. Zellhuber, C. Meraner, R. Kulkarni, B. Schuermans, and W. Polifke. Large Eddy Simulation of Flame Response to Transverse Acoustic Excitation in a Model Reheat Combustor. *Journal of Engineering for Gas Turbines and Power*, 2013, 135(9):091508/1-9.

[29] Ö. L. Gülder, G. J. Smallwood, R. Wong, D. R. Snelling, B. M. Deschamps, and J.-C. Sautet. Flame front surface characteristics in turbulent premixed propane/air combustion. *Combustion and Flame*, 2000, 120:407–416.

[30] S. Pfadler, F. Beyrau, and A. Leipertz. Flame front detection and characterization using conditioned particle image velocimetry (CPIV). *Optics Express*, 2007, 15:15444–15456.

[31] I. B. Celik, Z. N. Cehreli, and N. Yavuz. Index of resolution quality for Large Eddy Simulations. *Journal of Fluids Engineering*, 2005, 127:949–958.

[32] B. Schuermans, H. Luebcke, D. Bajusz, and P. Flohr. Thermoacoustic analysis of gas turbine combustion systems using unsteady CFD. In *Proceedings of the ASME Turbo Expo, GT2005-68393*, Reno, Nevada, 2005.

[33] L. Valino. A field monte carlo formulation for calculating the probability density function of a single scalar in a turbulent flow. *Flow, Turbulence and Combustion*, 1998, 60(2):157–172.

[34] R. Mustata, L. Valino, C. Jimenez, W. P. Jones, and S. Bondi. A probability density function Eulerian Monte Carlo field method for large eddy simulations: Application to a turbulent piloted methane/air diffusion flame (Sandia D). *Combustion and Flame*, 2005, 145(1-2):88–104.

[35] W. P. Jones, S. Navarro-Martinez, and O. Röh. Large eddy simulation of hydrogen auto-ignition with a probability density function method. *Proceedings of the Combustion Institute*, 2007, 31(2):1765–1771.

[36] W. P. Jones and S. Navarro-Martinez. Large eddy simulation of autoignition with a subgrid probability density function method. *Combustion and Flame*, 2007, 150:170–187.

[37] R. Kulkarni and W. Polifke. LES of Delft-Jet-In-Hot-Coflow (DJHC) with tabulated chemistry and stochastic fields combustion model. *Fuel Processing Technology*, 2013, 107:138–146.

[38] R. Kulkarni, M. Zellhuber, and W. Polifke. LES based investigation of autoignition in turbulent coflow configurations. *Combustion Theory and Modelling*, 2013, 17(2):224–259.

[39] A. Ni, W. Polifke, and F. Joos. Ignition delay time modulation as a contribution to thermoacoustic instability in sequential combustion. In P*roceedings of ASME Turbo Expo, 2000-GT-0103*, Munich, Germany, 2000. ASME.

[40] M. Zellhuber, B. Schuermans, and W. Polifke. Impact of acoustic pressure on auto-ignition and heat release. *Combustion Theory and Modelling, accepted for publication*, 2013.

[41] M. Zellhuber, V. Bellucci, B. Schuermans, and W. Polifke. Modelling the impact of acoustic pressure waves on auto-ignition flame dynamics. In *Proceedings of the European Combustion Meeting, ECM2011*, Cardiff, UK, 2011.

[42] P. J. Schmid, L. Li, M. P. Juniper, and O. Pust. Applications of the dynamic mode decomposition. *Theoretical Computational Fluid Dynamics*, 2011, 25:249–259.

[43] B. Schuermans, W. Polifke, and C. Paschereit. Modeling transfer matrices of premixed flames and comparison with experimental results. In *Proceedings of ASME Turbo Expo 1999, 99-GT-132*, 1999.

[44] U. Krüger, J. Hüren, S. Hoffmann, W. Krebs, P. Flohr, and D. Bohn. Prediction and measurement of thermoacoustic improvements in gas turbines with annular combustion systems. In *Proceedings of the ASME Turbo Expo 2000, 2000-GT-0084*, 2000.

[45] S. M. Camporeale, B. Fortunato, and G. Campa. A finite element method for three-dimensional analysis of thermo-acoustic combustion instability. *Journal of Engineering for Gas Turbines and Power*, 2010, 133(1):011506:1–13.

[46] A. Huber and W. Polifke. Dynamics of practical premix flames, part I: Model structure and identification. Int. *J. of Spray and Combustion Dynamics*, 2009, 1(2):199–229.

[47] L. Tay Wo Chong, T. Komarek, R. Kaess, S. Föller, and W. Polifke. Identification of flame transfer functions from LES of a premixed swirl burner. In *Proceedings of ASME Turbo Expo 2010, GT2010-22769*, 2010.

[48] M. K. Myers. Transport of energy by disturbances in arbitrary steady flows. *Journal of Fluid Mechanics*, 1991, 226:383–400.

[49] F. Nicoud and T. Poinsot. Thermoacoustic instabilities: Should the Rayleigh criterion be extended to include entropy changes? *Combustion and Flame*, July 2005, 142(1-2):153–159.

[50] A. Giauque. *Fonctions de Transfert de Flamme et Energies des Perturbations*

dans les Ecoulements Reactifs. PhD thesis, Institut National Polytechnique, Toulouse, 2007.

[51] K. Joseph George and R. I. Sujith. On Chu's disturbance energy. *Journal of Sound and Vibration*, October 2011, 330(22):5280–5291.

[52] K. Joseph George and R. I. Sujith. Disturbance energy norms: A critical analysis. *Journal of Sound and Vibration*, March 2012, 331(7):1552–1566.

[53] M. J. Brear, F. Nicoud, M. Talei, A. Giauque, and E. R. Hawkes. Disturbance energy transport and sound production in gaseous combustion. *Journal of Fluid Mechanics*, 2012, 707:53–73.

[54] J. Schwing and T. Sattelmayer. High-frequency instabilities in cylindrical flame tubes: Feedback mechanism and damping. In *Proceedings of ASME Turbo Expo 2013, GT2013-94064*, 2013.